

Integer Fluxonium Qubit

Raymond A. Mencia^{1,2}, Wei-Ju Lin², Hyunheung Cho², Maxim G. Vavilov³, and Vladimir E. Manucharyan^{1,2}

¹*Institute of Physics, Ecole Polytechnique Federale de Lausanne, 1015 Lausanne, Switzerland*

²*Department of Physics, Joint Quantum Institute, and Quantum Materials Center, University of Maryland, College Park, MD 20742, USA and*

³*Department of Physics, University of Wisconsin-Madison, Madison, WI 53562, USA*

(Dated: March 26, 2024)

We describe a superconducting qubit derived from operating a properly designed fluxonium circuit in a zero magnetic field. The qubit has a frequency of about 4 GHz and the energy relaxation quality factor $Q \approx 0.7 \times 10^7$, even though the dielectric loss quality factor of the circuit components is in the low 10^5 range. The Ramsey coherence time exceeds 100 μs , and the average fidelity of Clifford gates is benchmarked to $\mathcal{F} > 0.999$. These figures are likely to improve by an order of magnitude with optimized fabrication and measurement procedures. Our work establishes a ready-to-use “partially protected” superconducting qubit with the error rate comparable to the best transmons.

I. INTRODUCTION

In recent years, superconducting fluxonium qubits have reached [1–7] and may have even exceeded [8, 9] the state-of-the-art coherence time and gate error, defined by the industry-standard transmons [10–12]. Circuit-wise, the difference between the two devices seems minimal. A transmon is fundamentally a weakly anharmonic electromagnetic oscillator defined by a Josephson junction’s inductance and a shunting capacitance [10], while a fluxonium contains an additional high-inductance (superinductance) shunt, which nevertheless dramatically increases the qubit anharmonicity without introducing new decoherence channels [13–15]. The strongly anharmonic spectrum of fluxoniums is an important new resource for superconducting quantum processors, as it can help mitigate the propagation of coherent errors [16]. Another notable distinction is that fluxoniums operate at a much lower frequency, usually ranging around 100–1000 MHz, as opposed to the typically 4–6 GHz frequency range for transmons. In fact, given that the dielectric loss [17–20] is the primary decoherence mechanism in both devices, it is essentially the lower frequency of fluxoniums that allows matching the best transmons with far less sophisticated material science research and fabrication procedures [21–26].

Other ideas for post-transmon qubits are being actively explored. One direction is developing control techniques for even lower frequency fluxoniums [2, 27, 28] which are expected to have even longer coherence time, albeit not necessarily higher quality factor. The more sophisticated “protected” qubits can presumably have arbitrarily strong protection from any local decoherence source by operating at a nearly zero frequency [29–31]. However, these elegant ideas rely on a high degree of symmetry in the circuit Hamiltonians, which is challenging to implement with the present level of fabrication disorder [32, 33]. A more practical direction is exploring “partially protected” qubits [34], for example, qubits in the transmon frequency range that are to some degree decoupled from dielectric loss, such as the recently demonstrated “soft $0 - \pi$ ” [35] and bifluxon qubits [36]. Finally, a

significant effort is dedicated to hardware-efficient quantum error correction with bosonic codes, based on using transmons as switches rather than qubits, to control the quantum states of radiation in linear microwave cavities [37, 38]. Such schemes would likely benefit from substituting a transmon with a lower-error rate control device.

Here, we circle back to conventional fluxoniums and point out that they can equally well operate as relatively high-frequency qubits when biased at the less explored integer flux quantum sweet spot, as opposed to the usual half-integer flux quantum sweet spot. Circuit parameters must be adjusted such that the low-energy dynamics is governed entirely by flux quantization in the loop and is well described by the dual of the Cooper pair box Hamiltonian [39]. In this case, the lowest excited state is a doublet, originating from the classical degeneracy of charging an inductance L with a positive vs. a negative flux quantum at energy $(h/2e)^2/2L$. Tunneling splits the doublet. The lower doublet and the ground states define the integer fluxonium qubit, while the parity selection rule forbids the transition to the higher doublet state from the ground state. Such a doublet has been spectroscopically observed [13] and characterized in the time domain [15] in the very first fluxonium device. A more recently published study reports the observation of comparably long relaxation and coherence times, well in excess of 100 μs , at both sweet spots [40]. This work demonstrates that the doublet nature of the fluxonium transition at zero flux is compatible with precision single-qubit gates, the average fidelity of which is benchmarked to higher than 0.999. This benchmark is expected to improve by at least an order of magnitude if an active magnetic flux control is performed and with appropriate optimization of fabrication and measurement procedures. In the meantime, this result adds a ready-to-use device, nicknamed “integer fluxonium” qubit, to the relatively short list of high-performance superconducting qubits.

The paper is organized as follows. In section II we demonstrate the equivalence of the integer and the half-integer flux quantum sweet spots with respect to the energy relaxation rate using an elementary model of flux quantization

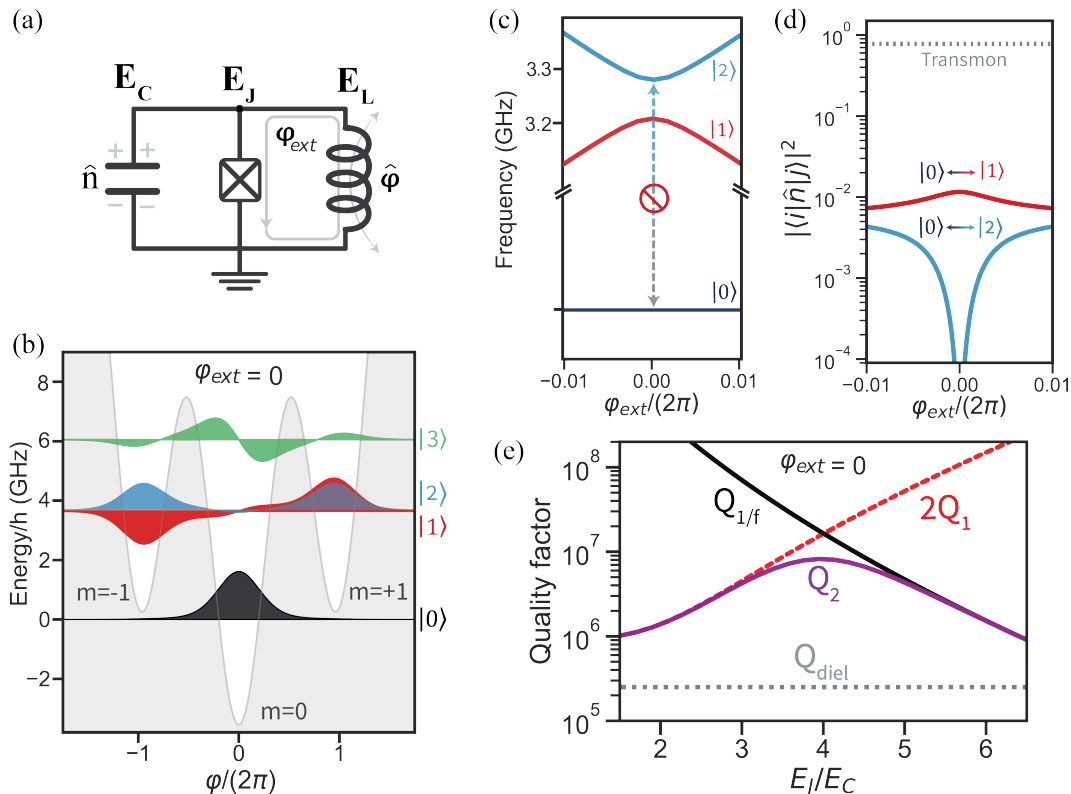


FIG. 1. (a) Fluxonium circuit model (see text). (b) An example of the effective potential energy profile in zero field superimposed on the lowest four energy states is Transition $|0\rangle\text{-}|1\rangle$ originates from tunneling between the local minima, and it defines the integer fluxonium qubit. The parity selection rule forbids the nearly degenerate transition $|0\rangle\text{-}|2\rangle$. Finally, transition $|0\rangle\text{-}|3\rangle$ corresponds to anharmonic oscillations in the lowest minima, and it is sufficiently detuned from the qubit. (c,d) Frequencies and charge matrix elements of the two lowest transitions calculated near zero field. (e) Illustration of the required balance between energy relaxation quality factor Q_1 and $1/f$ flux noise dephasing quality factor $Q_{1/f}$ for finding optimal integer fluxonium parameters. Given the experimental values of the $1/f$ flux noise amplitude $A_{1/f} = 1.4 \times 10^{-6}$ and the base dielectric loss quality factor $Q_{\text{diel}} = 2.5 \times 10^5$, there is an optimal value $E_J/E_C \approx 4$ that maximizes the qubit's total decoherence quality factor $Q_2 = (2Q_1^{-1} + Q_{1/f}^{-1})^{-1}$

in a superconducting loop. In section III we describe devices and data, including a complete case study for device D in Table 1. In section IV we share concluding remarks.

II. THEORY OF INTEGER FLUXONIUM

The fluxonium circuit (see Fig. 1a) is defined by three parameters: the Josephson energy E_J of the Josephson junction, the charging energy $E_C = e^2/2C$ of the total capacitance C and the inductive energy $E_L = (\hbar/2e)^2/L$ of the superinductance L . The junction and the inductance form a superconducting loop, which can be biased by an external magnetic flux $\varphi_{\text{ext}} \times (\hbar/2e)$. Quantum mechanics of fluxoniums is usually described by a pair of conjugate macroscopic variables, the superconducting phase-difference φ across the Josephson junction and the charge $2e \times n$. The two observables, the phase, $\hat{\varphi}$, and the Cooper pair number operator, \hat{n} , displaced at the capacitor satisfy the standard position-momentum-like commu-

tation relation $[\hat{\varphi}, \hat{n}] = i$ and the Hamiltonian reads

$$H = 4E_C \hat{n}^2 + \frac{1}{2} E_L \hat{\varphi}^2 - E_J \cos(\hat{\varphi} - \varphi_{\text{ext}}). \quad (1)$$

The parameter regime for integer fluxonium is derived from the following arguments. First, as with all fluxoniums, it is essential to have $E_L \ll E_J$, in which case the potential energy (the φ -dependent term of Eq. (1)) has multiple local minima (Fig. 1b). The charging energy term is equivalent to the kinetic energy of a particle with a mass C moving in such a potential. There are two types of excitations: oscillations in a single well (plasmon) and tunneling between the wells (fluxon). One must decouple these excitations to implement integer fluxonium, which is achieved by setting the plasmon frequency sufficiently above the fluxon frequency. In the asymptotic limit of weak tunneling, that is $E_J/E_C \gg 1$, the plasmon energy is given approximately by $\sqrt{8E_J E_C}$ while the fluxon energy is approximately $2\pi^2 E_L$, which reduces the parameter requirement for the integer fluxonium to $\sqrt{8E_J E_C} \gg 2\pi^2 E_L$, with qubit frequency given

approximately by $\hbar\omega_{01} \approx 2\pi^2 E_L$, the offset between the lowest two potential wells in Fig. 1b.

A. Flux-dual Cooper pair box model

Although spectral properties of integer fluxonium can be calculated numerically from the Hamiltonian (1) for arbitrary circuit parameters and flux bias (see Fig. 1c,d), it is insightful to consider an effective model defined entirely in terms of flux quantization and tunneling [14, 41]. We start with the basis of fluxon states $|m\rangle$ corresponding to a particle resting at the bottom of the m -th Josephson well (in reality, we are only interested in the lowest three wells shown in Fig. 1a). Introducing the phenomenological tunneling energy amplitudes ϵ_1 to change m by ± 1 and ϵ_2 to change m by ± 2 we can write the following effective Hamiltonian

$$H_{\text{eff}} = \sum_m \frac{E_L^\Sigma}{2} (2\pi m - \varphi_{\text{ext}})^2 |m\rangle\langle m| + \frac{\epsilon_1}{2} \sum_m |m\rangle\langle m \pm 1| + \frac{\epsilon_2}{2} \sum_m |m\rangle\langle m \pm 2|, \quad (2)$$

where $E_L^\Sigma = (E_L^{-1} + E_J^{-1})^{-1}$ and is the total linearized loop inductance. The values of the tunneling amplitudes ϵ_1 and $\epsilon_2 \ll \epsilon_1$ depend on the three circuit parameters E_J , E_C , and E_L , but it is safe to assume that both amplitudes are exponentially suppressed with the parameter $\sqrt{8E_J/E_C}$. The double-fluxon tunneling amplitude ϵ_2 is not necessary to derive the main properties of integer fluxonium. Still, it is necessary to obtain an accurate value of ϵ_1 by matching the low-energy spectra of the two Hamiltonians (1,2). In fact, for $\epsilon_2 = 0$, the Hamiltonian (2) describes a Cooper pair box (a charge qubit) in the regime of strong charge quantization, where charging energy is replaced by the inductive energy, Cooper pairs with fluxons, and offset charge with the flux bias.

The spectrum of the model Hamiltonian (2) near zero bias can be obtained by diagonalizing the corresponding 3×3 matrix in the basis of three fluxon states $|m = -1\rangle$, $|m = 0\rangle$, and $|m = +1\rangle$. Setting $\varphi_{\text{ext}} = 0$ in Eq. 2 and introducing a small parameter $\alpha = \epsilon_1/4\pi^2 E_L^\Sigma$ we get the following perturbative expressions for the three lowest-energy eigenstates:

$$\begin{aligned} |0\rangle &= |m = 0\rangle + \alpha(|m = -1\rangle + |m = +1\rangle), \\ |1\rangle &= \frac{1}{\sqrt{2}}(|m = -1\rangle - |m = +1\rangle), \\ |2\rangle &= \frac{1}{\sqrt{2}}(|m = -1\rangle + |m = +1\rangle) - \sqrt{2}\alpha|m = 0\rangle. \end{aligned} \quad (3)$$

The eigenstates $|1\rangle$ and $|2\rangle$ define the excited-state doublet of integer fluxonium. The two transition frequencies are given by $\hbar\omega_{01} = 2\pi^2 E_L^\Sigma + \alpha\epsilon_1 - \epsilon_2/2$ and $\hbar\omega_{02} = 2\pi^2 E_L^\Sigma + 2\alpha\epsilon_1 + \epsilon_2/2$. Thus, the doublet is split by $\hbar\omega_{12} = \alpha\epsilon_1 + \epsilon_2$. Note that ϵ_2 parameter does not affect the eigenstates but merely increases the doublet

splitting ω_{12} . In the qualitative analysis below, we will set ϵ_2 to zero to simplify the expressions without losing the essence.

The matrix elements of $\hat{\varphi}$ and \hat{n} operators can be obtained by noting the relation $\hat{\varphi} = 2\pi\hat{m}$ and using the identity $\langle i|\hat{n}|j\rangle = \langle i|\hat{\varphi}|j\rangle \times (\hbar\omega_{ij}/8E_C)$, which follows directly from the commutation rule and Eq. (1). For the phase-difference matrix elements, we get $\langle 0|\hat{\varphi}|2\rangle = 0$ and $\langle 0|\hat{\varphi}|1\rangle \approx 2\pi\alpha \ll 1$. Note, in case of a conventional fluxonium operation at $\varphi_{\text{ext}} = \pi$, within the model of Eq. (2), we have $\hbar\omega_{01} = \epsilon_1$ and $\langle 0|\hat{\varphi}|1\rangle \approx \pi$, which is a much larger number than at the integer flux bias. Yet, the matrix elements of the conjugate Cooper pair number operator \hat{n} come out essentially the same at the two sweet spots:

$$\langle 0|\hat{n}|1\rangle_{\varphi_{\text{ext}}=0} \approx \sqrt{2}\langle 0|\hat{n}|1\rangle_{\varphi_{\text{ext}}=\pi} \approx \frac{\sqrt{2}\pi}{8} \frac{\epsilon_1}{E_C}. \quad (4)$$

The degree of protection of integer fluxonium from energy relaxation can be judged by comparing this matrix element estimate with the typical transmon value, $\sqrt[4]{E_J/8E_C} \simeq 1$ [42].

The above qualitative analysis based on Eq. (2) complements accurate numerical calculations based on Eq. 1. Examples of calculated wave functions, transition frequencies, and matrix elements are shown in Fig. (1b-d). More importantly, the plasmon transition enables a dispersive qubit-cavity interaction used for the qubit read-out, as long as the cavity frequency is not too far detuned from the plasmon [43].

B. Dielectric loss vs. 1/f flux noise

An optimal design for an integer fluxonium must simultaneously suppress the effect of the two prevailing decoherence mechanisms: the dielectric loss and the 1/f flux noise. Both channels originate from defects in the surface oxide layers of superconducting leads and thus cannot be readily eliminated, at least not in the near future. Let us define the dielectric loss via the effective loss tangent $\tan \delta_C$ of the circuit's total capacitance C [44–46]. For both transmon and fluxonium qubits, the energy relaxation quality factor Q_1 is related to Q_{diel} according to the expression of Fermi's Golden rule $Q_1 = \omega_{01}T_1$, and $1/T_1 = E_C \times 32\pi |\langle 0|\hat{n}|1\rangle|^2/Q_{\text{diel}}$, where we define $Q_{\text{diel}} = 1/\tan \delta_C$ as the effective dielectric loss quality factor. For a transmon, $Q_1 = Q_{\text{diel}}$. For the best transmons, $Q_{\text{diel}} \approx 1.5 \times 10^7$ [47–49]. For integer fluxonium, we can qualitatively estimate the parameter dependence of Q_1 as

$$Q_1 \propto \frac{E_C}{\hbar\omega_{12}} \times Q_{\text{diel}}. \quad (5)$$

To estimate the dephasing rate due to the 1/f flux noise, we define the noise spectral density as $S_{1/f}(\omega) = 2\pi A_{1/f}^2 \times (h/2e)^2/\omega$, where the quantity $A_{1/f}$ characterizes the strength of the flux noise. Slow variation

in the value of φ_{ext} induces a slow variation of the qubit frequency to second order in the value of $A_{1/f}$ and proportionally to the curvature of the qubit transition with respect to the flux bias, that is $d^2\omega_{01}/d\varphi_{\text{ext}}^2$ at $\varphi_{\text{ext}} = 0$. The resulting pure dephasing quality factor $Q_{1/f} = \omega_{01}T_{1/f}$ is given up to a numerical factor:

$$Q_{1/f} \propto \frac{\hbar\omega_{12}}{E_L} \times \frac{1}{A_{1/f}^2}. \quad (6)$$

Reducing the frequency ω_{12} would increase Q_1 but reduce $Q_{1/f}$ by the same amount, without changing the qubit transition frequency $\hbar\omega_{01} \approx 2\pi^2 E_L$. The combined decoherence quality factor $Q_2 = 1/(1/2Q_1 + 1/Q_{1/f})$ reaches its maximum for a specific value of E_J/E_C , which depends on the experimental values of Q_{diel} and $A_{1/f}$. In other words, the strength of flux noise $A_{1/f}$ determines how much the qubit's quality factor can be increased over the dielectric loss limit Q_{diel} . Fig. 1e illustrates the described balance using experimentally motivated values of $A_{1/f} = 10^{-6}$ and $Q_{\text{diel}} = 2.5 \times 10^5$, resulting in an enhancement factor as large as $Q_2/Q_{\text{diel}} \approx 40$.

C. Leakage to state $|2\rangle$

The more integer fluxonium is made protected from energy relaxation, the smaller the splitting between the computational level $|1\rangle$ and the non-computational level $|2\rangle$. As long as $\varphi_{\text{ext}} = 0$, no leakage to state $|2\rangle$ is expected during qubit manipulations. Indeed, a resonant qubit drive at a frequency around ω_{01} does not couple to transition $|0\rangle$ - $|2\rangle$ because $\langle 0|\hat{n}|2\rangle = 0$, nor does it couple to transition $|1\rangle$ - $|2\rangle$ because of the large frequency detuning. Thus, in theory, integer fluxonium is effectively a 2-level system: even transition $|0\rangle$ - $|3\rangle$ would not be coupled by the drive because of its large detuning.

In practice, though, there is always a small deviation $\delta\varphi_{\text{ext}} \ll 1$ of the value φ_{ext} from an integer value, either due to an instrument imprecision, or a background field, or at the very least due to the same $1/f$ flux noise that causes pure dephasing. Consequently, the qubit drive acquires a small coupling to state $|2\rangle$, proportional to the value of $(d\langle 0|\hat{n}|2\rangle/d\varphi_{\text{ext}})\delta\varphi_{\text{ext}}$ near $\varphi_{\text{ext}} = 0$. The frequencies ω_{01} and ω_{02} would also be slightly shifted to the second order in $\delta\varphi_{\text{ext}}$. For a given $\delta\varphi_{\text{ext}}$, we can model the resulting coherent errors in our qubit using the following elementary 3-level Hamiltonian

$$H_{\text{drive}}(\delta\varphi_{\text{ext}})/\hbar = \omega_{01}|1\rangle\langle 1| + \omega_{02}|2\rangle\langle 2| + \hat{n} \times (I(t) \cos \omega t + Q(t) \sin \omega t), \quad (7)$$

where $\omega \approx \omega_{01}$ and $I(t)$ and $Q(t)$ are slowly varying envelopes defining the qubit pulse shape. We use a numerical solution of this Hamiltonian to interpret the results of randomized benchmarking of experimental devices.

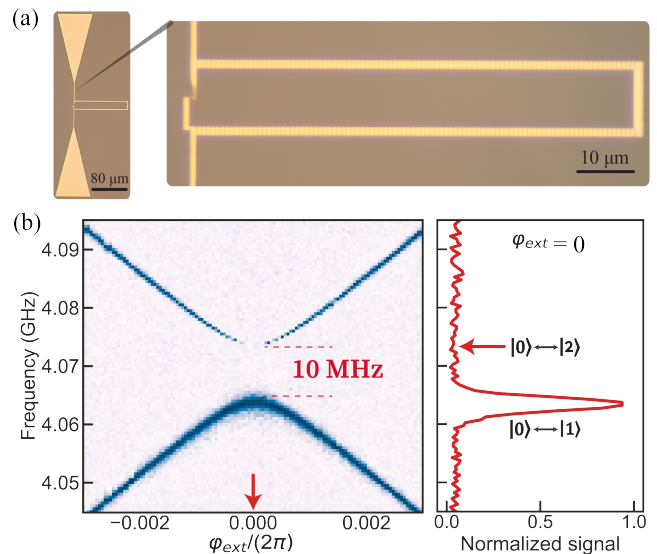


FIG. 2. (a) Optical image of integer fluxonium device. (b) Two-tone spectroscopy signal (arbitrary units) as a function of frequency and flux bias near $\varphi_{\text{ext}} = 0$. Inset shows a cross-section at $\varphi_{\text{ext}} = 0$. Note the absence of the $|0\rangle$ - $|2\rangle$ within the given signal-to-noise ratio.

III. QUBIT CHARACTERIZATION

A. Spectroscopy and decoherence

Spectroscopy and time-domain data were collected on four different devices. The device parameters are extracted from fitting the model in Eqs. (1) and (2) and are summarized in Table 1. In comparison to Ref. [1], we increased the charging energy E_C and the Josephson energy E_J but reduced the inductive energy E_L . Similarly to Ref. [8], the readout is performed using a capacitive coupling to a 3D cavity for samples A, B, and D. Sample C was coupled inductively to an on-chip resonator and read out using a wireless coupling to a 3D waveguide, similarly to Ref. [50–52]. Fabrication and measurement procedures are similar to those in Ref. [1].

Figure 2a shows an optical image of device A, reminiscent of fluxonium devices from Ref. [53] except with a smaller antenna part. Fig. 2b shows the spectrum of device D near $\varphi_{\text{ext}} = 0$. The data reveals a doublet analogous to the one first observed in Refs. [13, 54], except the splitting at $\varphi_{\text{ext}} = 0$ is reduced to a mere 11 MHz. The inhibition of transition $|0\rangle$ - $|2\rangle$ is illustrated in the inset of Fig. 1b. The transition $|0\rangle$ - $|3\rangle$ is above 5 GHz. This device's calculated Cooper pair number transition matrix element is $\langle 0|\hat{n}|1\rangle \approx 0.056$ and is at least an order of magnitude below the typical transmon value.

Energy relaxation time T_1 shows a negligible flux dependence (Fig. 3c) as the qubit frequency is increased by an order of magnitude from its half-integer flux value of $\omega_{01}/2\pi = 190$ MHz to the integer flux bias value of $\omega_{01}/2\pi = 3450$ MHz. Interleaved measurements of T_1

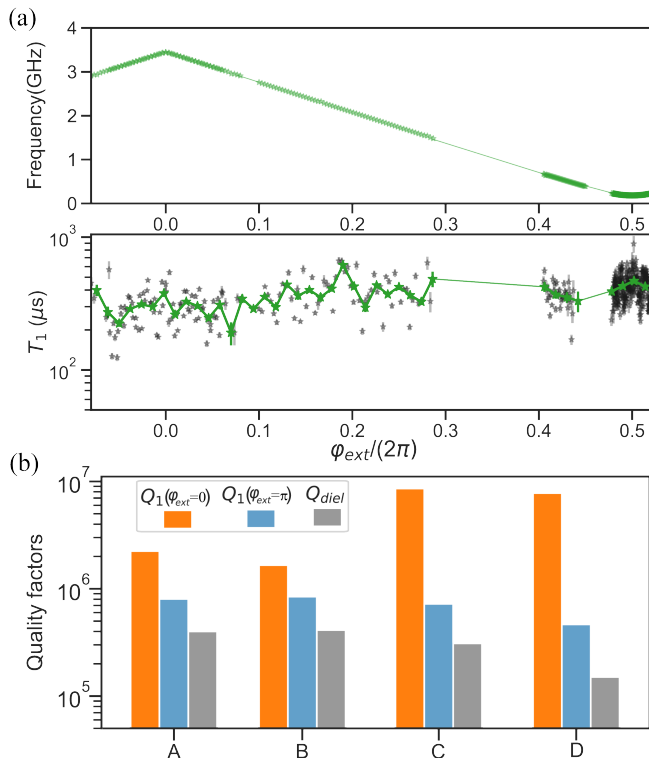


FIG. 3. (a) The experimentally measured transition frequencies (top) and energy relaxation times (bottom) of sample C as a function of external flux bias. The average values of T_1 are shown in green. (b) The quality factor of the measured qubit transitions due to energy relaxation, Q_1 , at each flux sweet spot along with the extracted value of Q_{diel} .

and T_2^E were done extensively over many hours to probe the repeatability of each characteristic time. We obtain the respective average times shown in Table 1 as \bar{T}_1 and \bar{T}_2^E by averaging each individual fit of the respective measurements. The energy relaxation quality factors $Q_1 = \omega_{01}T_1$ are compared for each device at $\varphi_{\text{ext}} = 0, \pi$ as well as with the extracted value of Q_{diel} (Fig. 3b). We highlight that the measured quality factor in devices C and D are in the $Q_1 \simeq (6.5 - 7.0) \times 10^6$ range. Not only is this number within a factor of two from the highest Q reported for optimally fabricated transmons [26], but the dielectric quality factor for these devices is in the low 10^5 range. Frequency dependence of T_1 in multiple devices seems consistent with the dielectric loss model (Fig. 7). Nevertheless, our experiment cannot exclude other energy relaxation channels, so the estimation of the Q_{diel} should be taken as an upper bound.

The coherence in samples A and B was limited by energy relaxation, as indicated by $T_2^E \approx 2T_1 \approx 200 \mu\text{s}$. The coherence time in devices C, D is most likely limited by cavity photon shot noise. In case of sample D we describe a more accurate measurement of the uncorrected Ramsey coherence time T_2^* in the vicinity of the sweet spot $\varphi_{\text{ext}} = 0$ (see Fig. 4). We find that the flux dependence away from the sweet spot is consistent with

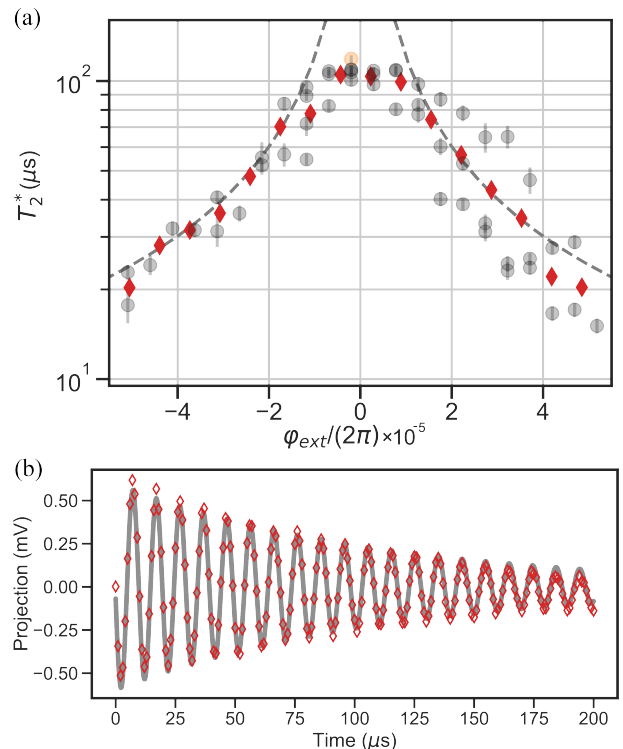


FIG. 4. (a) The Ramsey coherence time T_2^* of device D as a function of external flux. Dashed line is the first-order theoretical value with $A_{1/f} \approx 1.4 \times 10^{-6}$. (b) Example Ramsey fringe measured at $\varphi_{\text{ext}} = 0$; corresponding to the orange data point in (a).

the $1/f$ flux noise with the amplitude $A_{1/f} \approx 1.4 \times 10^{-6}$, which is similar to what was measured in previous fluxonium experiments. The value of T_2^* saturates at about $T_2^* \approx 100 \mu\text{s}$ in an interval $|\varphi_{\text{ext}}|/2\pi < 10^{-5}$. From this measurement, we conclude that the short-term stability of the flux bias in an integer fluxonium device can be on the order of $\delta\varphi_{\text{ext}}/2\pi < 10^{-5}$.

B. Gates benchmarking

We arrive at the most important demonstration of the potential usefulness of integer fluxonium, benchmarking of the single-qubit Clifford-group gates. This test is especially critical due to the possibility of the state- $|2\rangle$ leakage under an imperfect integer flux quantum bias. For benchmarking, we select device D as the most protected and, hence, most potentially sensitive to the leakage.

The experimentally performed RB sequence consists of randomly chosen Clifford gates applied to the qubit before applying a single inversion gate; bringing the state back to the initial. The number of Clifford gates before the final state inversion gate is increased, resulting in a decaying probability of properly recovering the initial state. Measurements are fit according to the polynomial $A + Bp^m$; where p is the depolarization parameter while

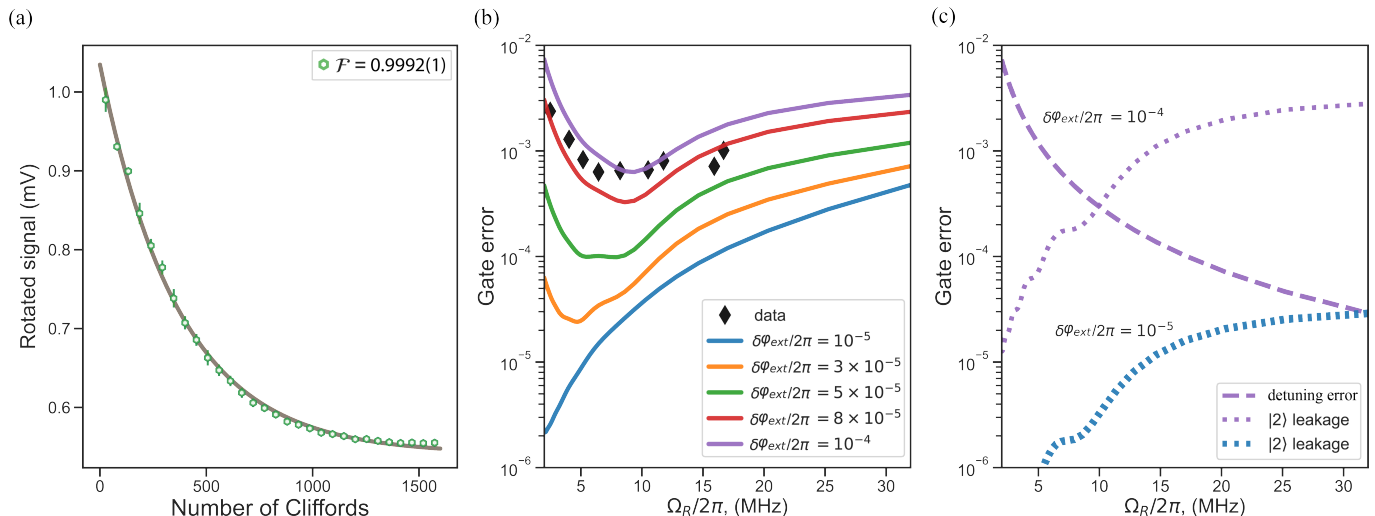


FIG. 5. (a) The RB trace for optimal fidelity $\mathcal{F} = 99.92 \pm .01\%$ measured at a Rabi frequency of 6 MHz. (b) RB measurements for different Rabi frequencies (black diamonds) superimposed with the gate errors expected based on small flux offsets, $\delta\varphi_{\text{ext}}/2\pi$. The gate error due to flux offsets does not dominate until about $\delta\varphi_{\text{ext}}/2\pi = 10^{-4}$. (c) The Rabi-phase error (dashed line) and the $|2\rangle$ leakage (dotted line) combine to produce the error fidelity. Here, each separate contribution is shown.

A and B are constants that account for state preparation and measurement (SPAM) errors [55]. The average error rate $1 - \mathcal{F}$ for Clifford group gates is defined as $(1 - \mathcal{F}_{\text{Cliff}}) = (1 - p)/2$. Since there are on average 1.833 physical gates per Clifford the average physical gate fidelity is $(1 - \mathcal{F}) = (1 - \mathcal{F}_{\text{Cliff}})/1.833$ [7, 8]. The best average physical gate fidelity measured was $\mathcal{F} = 0.9992(1)$ (Fig. 5a) with a Rabi frequency of $\Omega_{\text{Rabi}} = 6.2$ MHz.

C. Leading errors

Randomized benchmarking measurements for sample D are then simulated in QuTip [56] to quantify different contributing sources of error. The simulation uses smooth-edged pulses with a switching on/off time of 5 ns to evaluate the full evolution operator U at the end of the pulse. The theoretical estimate of the fidelity is obtained from [57]

$$\mathcal{F} = \frac{\text{Tr}(U_{\text{comp}}^\dagger U_{\text{comp}}) + |\text{Tr}(U_{\text{comp}}^\dagger U_{\text{ideal}})|^2}{6},$$

where U_{comp} is the evolution operator projected to the computational subspace. We find the primary source limiting the experimental gate fidelity is best described by a model assuming that a small static flux detuning (on the order of $\Phi_0 \times 10^{-5}$) away from $\varphi_{\text{ext}} = 0$ is developed after the gates were calibrated. The origin of this offset is probably related to an imperfect shielding of our experiment from external stray magnetic fields. The flux offset produces a non-zero $|0\rangle - |2\rangle$ matrix element and can therefore enhance leakage for large Rabi frequencies. We evaluate the leakage error to state $|2\rangle$ in terms

of the matrix elements of the full evolution operator as $\varepsilon_{\text{leak}} = (|U_{02}|^2 + |U_{12}|^2)/2$. The results of this estimation for the flux detuning $\delta\varphi_{\text{ext}}/2\pi = 10^{-4}$ and 10^{-5} are shown in Fig. 5c.

Furthermore, if flux-detuning occurs after excitation pulse calibration, the pulse no longer provides a perfect rotation. We focus on the X gate when $U_{\text{ideal}} = \sigma_x$. In this case, the gate error without leakage can be estimated as $\varepsilon_{\text{det}} = 1 - \mathcal{F} = 2(1 - |U_{01}|^2)/3$. We estimate the magnitude of $|U_{01}|^2$ using the expression for the amplitude of the Rabi oscillations with detuning $\delta\omega_{01} = \omega_{01}(\delta\varphi_{\text{ext}}) - \omega_{01}(0)$ and obtain the error associated with the detuning of the transition frequency $\varepsilon_{\text{det}} = (8/3)(\delta\omega_{01}/2\pi)^2 t_g^2$ for the gate time t_g . The change in qubit frequency due to the flux offset can be approximated by $\delta\omega_{01}/2\pi = 8\pi^2 \langle 0|\hat{\varphi}|1\rangle E_L \delta\varphi_{\text{ext}}/2$ which is on the order of hundreds of kHz for sample D with $\delta\varphi_{\text{ext}}/2\pi = 10^{-4}$. The summation of the two error sources for each static flux offset is shown in Fig. 5b. These two errors scale inversely to one another as a function of Rabi frequency as illustrated in Fig. 5c for flux offset $\delta\varphi_{\text{ext}}/2\pi$.

Our RB results indicate that the gate error is not currently limited by the qubit coherence instead we find that small external flux offsets after parameter optimization at φ_{ext} produces a Rabi-phase error due to the nonperfect gate calibration at low Rabi frequency; while at large Rabi frequency the error is produced by the non-zero matrix element for $|0\rangle - |2\rangle$. Interestingly, the leakage to the second eigenstate is negligible for an external flux offset less than $\delta\varphi_{\text{ext}}/2\pi < 10^{-5}$ supporting the idea that the leakage into the closely situated state $|2\rangle$ is not an issue for perfect flux biasing at $\varphi_{\text{ext}} = 0$. In future exper-

	Sample	A	B	C	D
Fluxonium model fit	E_J (GHz)	4.12	3.84	7.20	6.86
	E_C (GHz)	1.64	1.75	2.04	1.46
	E_L (GHz)	0.18	0.14	0.18	0.23
Flux tunneling model fit	E_L^{Σ} (GHz)	0.172	0.135	0.175	0.222
	ϵ_1 (MHz)	308	362	190	91
	ϵ_2 (MHz)	73	81	6	9
Measured parameters	$\omega_{01}/2\pi$ (GHz)	3.20	2.51	3.45	4.14
	$\omega_{12}/2\pi$ (MHz)	103	106	24	11
	\bar{T}_1 (μ s)	109	101	328	255
	\bar{T}_2^E (μ s)	175	201	81	185
	\bar{T}_2^* (μ s)	38	61	57	118
	Inferred parameters	$Q_{\text{dielectric}}$	3.5×10^5	3.6×10^5	2.6×10^5
	$ n_{01} ^2$ (IFQ)	2.12×10^{-2}	1.85×10^{-2}	4.4×10^{-3}	3.2×10^{-3}

TABLE I. A summary of integer fluxonium device parameters. All measured parameters were performed while $\varphi_{\text{ext}} = 0$.

iments, the static offset can be eliminated by carefully removing all components producing magnetic noise close to the device.

IV. CONCLUSIONS

Integer fluxonium qubit operates in zero magnetic field and in the same frequency range as transmons, it has a comparably high quality factor and gate fidelity, despite a much lower quality of the circuit dielectrics. The degree of decoupling from the dielectric loss and similar relaxation mechanisms is controlled by the Cooper pair number matrix element $\langle 0|\hat{n}|1\rangle$, the value of which can be user-defined by adjusting the ratio E_J/E_C , independently of the qubit frequency.

The only catch of the integer fluxonium design is the presence of the second transition $|0\rangle\text{-}|2\rangle$ close to the qubit transition $|0\rangle\text{-}|1\rangle$, which can get activated by the qubit drive due to a slight deviation in the flux bias from zero or the integer flux quantum. So far, we demonstrated that even in a relatively extreme case of $\omega_{12}/2\pi = 11$ MHz (device D) and a relatively large flux offset of $\delta\varphi_{\text{ext}}/2\pi \sim 10^{-4}$, the gate error remains under 0.1% with about 10-20 MHz Rabi rate (π -pulse duration of 50-25 ns). Future experiments will reveal the practical limits to the flux-bias accuracy. We envision that the flux offset can be reduced to $\delta\varphi_{\text{ext}}/2\pi \lesssim 10^{-5}$ by either improved magnetic field shielding or an active feedback. Furthermore, due to the strong anharmonicity of the non-computational transitions, the leakage to state $|2\rangle$ may not be as dangerous as in transmons: the system remains contained to only three states $|0\rangle$, $|1\rangle$, and $|2\rangle$, and the system can be efficiently reset back to the computational subspace.

Fundamentally, the mechanism of decoupling of the integer fluxonium’s transition from energy relaxation is precisely the same as in the case of a regular low-frequency fluxonium, namely the suppression of the matrix element $\langle 0|\hat{n}|1\rangle$ far below the transmon’s value for the flux tunneling (fluxon) transition. This observation

calls for two important remarks. First, a Cooper pair box (charge qubit) device operated at zero offset gate charge could have been operated in the same manner as integer fluxonium were it not for the excessively high level of background charge noise felt by a typical superconducting island in comparison to the background flux noise felt by a typical superconducting loop. Second, integer fluxonium shares many common characteristics with the recently demonstrated “soft $0 - \pi$ ” qubit [35]. Both devices have a doublet qubit transition, leading to suppressed matrix elements of the flux and charge operators, combined with a first-order insensitivity to flux noise. It has been previously conjectured that achieving such a portfolio of properties requires a circuit with more than one degree of freedom [33]. Indeed, the “soft $0 - \pi$ ” qubit is constructed by a relatively strong coupling of three modes: fluxonium-like, transmon-like, and harmonic oscillator. By contrast, integer fluxonium is described by a single degree of freedom. Understanding the profound difference between the two devices in terms of the origins of the noise decoupling could lead to new ideas for high-performance qubit designs.

ACKNOWLEDGMENTS

We wish to acknowledge fruitful conversations with Chen Wang. This research was supported by the ARO HiPS (contract No. W911-NF18-1-0146) and GASP (contract No. W911-NF23-10093) programs.

Appendix A: Fluxonium numerics

The general fluxonium Hamiltonian is expressed as:

$$H = 4E_C\hat{n}^2 + \frac{1}{2}E_L\hat{\varphi}^2 - E_J\cos(\hat{\varphi} - \varphi_{\text{ext}}) \quad (\text{A1})$$

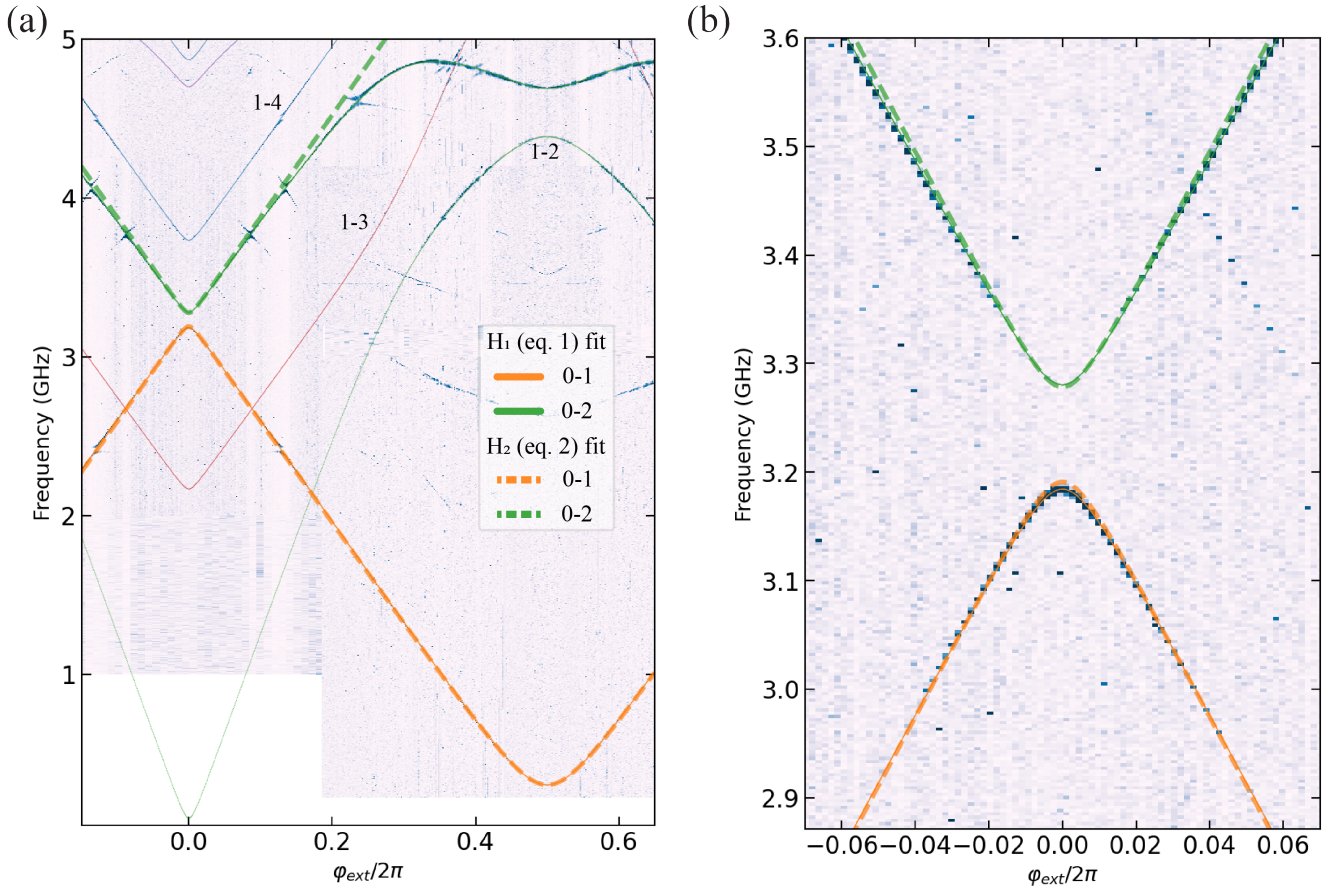


FIG. 6. (a) The two-tone spectroscopy of sample A superimposed with the fluxonium Hamiltonian (eq. 1, solid lines) and the effective Hamiltonian (eq. 2, dashed lines) fits. The thin lines correspond to transitions from the first excited state and are fit using the fluxonium Hamiltonian. (b) A zoom-in around $\varphi_{\text{ext}} = 0$ of the first two transitions plus both fits to demonstrate the high-degree of agreeability between the measured data and the two models.

The phase, $\hat{\varphi}$, and the Cooper pair number, \hat{n} , operators are expressed in the harmonic oscillator basis:

$$\begin{aligned}\hat{\varphi} &= \frac{1}{\sqrt{2}} \left\{ \frac{8E_C}{E_L} \right\}^{1/4} (a^\dagger + a), \\ \hat{n} &= \frac{i}{\sqrt{2}} \left\{ \frac{E_L}{8E_C} \right\}^{1/4} (a^\dagger - a)\end{aligned}\quad (\text{A2})$$

here a, a^\dagger are the harmonic oscillator raising and lower operators each with a Hilbert space dimension exceeding fifty oscillator states.

After numerical diagonalization, the eigenvalues of the fluxonium Hamiltonian are returned; however, the eigenfunctions are the coefficients necessary to construct the fluxonium wavefunctions by the linear superposition of harmonic oscillator wavefunctions defined as:

$$\psi_k(\varphi) = \frac{1}{(2\pi\varphi_{\text{zpf}}^2)^{1/4}} \frac{1}{\sqrt{2^k k!}} H_k(\varphi/\varphi_{\text{zpf}}) e^{-\varphi^2/4\varphi_{\text{zpf}}^2}, \quad (\text{A3})$$

where k is the integer index of the harmonic oscillator state and $\varphi_{\text{zpf}} = (8E_C/E_L)^{1/4}$. Using these wavefunctions with the coefficients found by diagonalization we

write $\Psi_j(\varphi) = \sum_{k=0}^{K} c_k \psi_k(\varphi)$, where c_k is the k th component of the eigenvector for the j th eigenstate after diagonalizing and $\sum_k |c_k|^2 = 1$.

Appendix B: Auxiliary data

The experimental spectra for each device was fit using both the conventional fluxonium Hamiltonian Eq. (1) and the discrete flux Hamiltonian Eq. (2). Extracted parameters from both fit models for each device is summarized in Table 1. The spectrum of qubit sample A is shown in Fig. 6. The fits to spectroscopy data show a near-perfect agreement of the fluxonium to the fluxon fit up to the vicinity of the plasmon. The comparison of the fits verified that all samples f_{01}^{IFQ} were indeed less than the plasmon mode frequency. The first two transitions show a sharp external flux dependence at integer flux values (Fig 6b). The larger the E_J/E_C ratio, the smaller the $|1\rangle \rightarrow |2\rangle$ frequency. The $|0\rangle - |2\rangle$ transition has a vanishing matrix element at IFQ and hence cannot be excited and is experimentally revealed by the two-tone

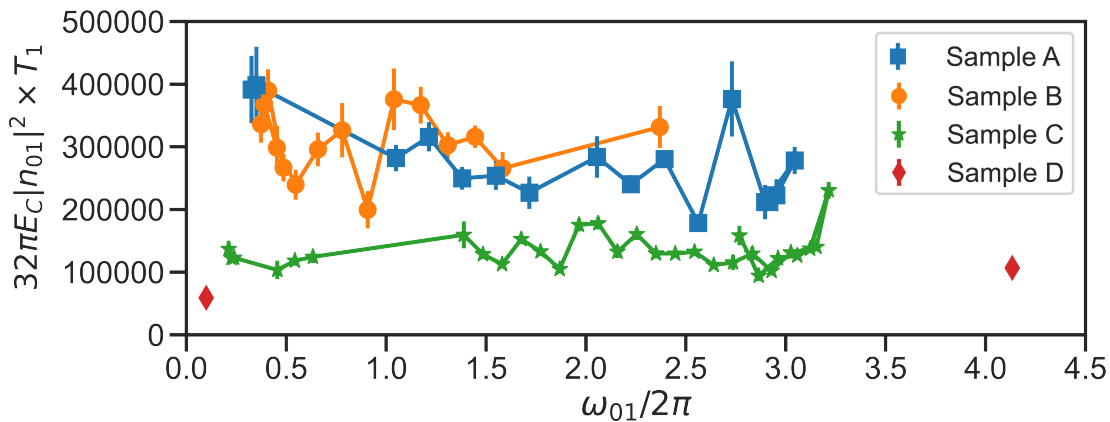


FIG. 7. The quantity $32\pi E_C |n_{01}|^2 \times T_1$ vs. the qubit frequency for four devices (see Table 1). The trend for frequency-independence over several octaves of frequency is consistent with the dielectric loss model. Data for devices A-C was compiled from Ref. [40]

signal vanishing at $\varphi_{\text{ext}} = 0$.

To further characterize qubits, T_1 was measured several times across half a flux quantum period for samples A-C; sample D was only measured at both sweet spots. Per sample, the multiple energy relaxation traces were first fit individually and were then binned together. The average decay constant per bin is the reported T_1 while the standard deviation per bin is the error. The binned

statistics of energy relaxation times were then converted into an effective Q_{diel} using Fermi's golden rule at zero temperature ($32\pi E_C |n_{01}|^2 \times T_1$). The results are shown in Fig. 7 versus the qubit transition frequency and illustrate the effective Q_{diel} does not depend explicitly on the qubit transition frequency. We note that incorporating a finite temperature to the lossy dielectric would only further increase the quality factor.

-
- [1] L. B. Nguyen, Y.-H. Lin, A. Somoroff, R. Mencia, N. Grabon, and V. E. Manucharyan, High-coherence fluxonium qubit, *Physical Review X* **9**, 041041 (2019).
- [2] H. Zhang, S. Chakram, T. Roy, N. Earnest, Y. Lu, Z. Huang, D. Weiss, J. Koch, and D. I. Schuster, Universal fast-flux control of a coherent, low-frequency qubit, *Physical Review X* **11**, 011010 (2021).
- [3] Q. Ficheux, L. B. Nguyen, A. Somoroff, H. Xiong, K. N. Nesterov, M. G. Vavilov, and V. E. Manucharyan, Fast logic with slow qubits: microwave-activated controlled-z gate on low-frequency fluxoniums, *Physical Review X* **11**, 021026 (2021).
- [4] H. Xiong, Q. Ficheux, A. Somoroff, L. B. Nguyen, E. Dogan, D. Rosenstock, C. Wang, K. N. Nesterov, M. G. Vavilov, and V. E. Manucharyan, Arbitrary controlled-phase gate on fluxonium qubits using differential ac stark shifts, *Physical Review Research* **4**, 023040 (2022).
- [5] F. Bao, H. Deng, D. Ding, R. Gao, X. Gao, C. Huang, X. Jiang, H.-S. Ku, Z. Li, X. Ma, *et al.*, Fluxonium: An alternative qubit platform for high-fidelity operations, *Physical Review Letters* **129**, 010502 (2022).
- [6] I. N. Moskalenko, I. A. Simakov, N. N. Abramov, A. A. Grigorev, D. O. Moskalev, A. A. Pishchimova, N. S. Smirnov, E. V. Zikiy, I. A. Rodionov, and I. S. Besedin, High fidelity two-qubit gates on fluxoniums using a tunable coupler, *npj Quantum Information* **8**, 130 (2022).
- [7] A. Somoroff, P. Truitt, A. Weis, J. Bernhardt, D. Yohannes, J. Walter, K. Kalashnikov, M. Renzullo, R. A. Mencia, M. G. Vavilov, *et al.*, Fluxonium qubits in a flip-chip package, *Physical Review Applied* **21**, 024015 (2024).
- [8] A. Somoroff, Q. Ficheux, R. A. Mencia, H. Xiong, R. Kuzmin, and V. E. Manucharyan, Millisecond coherence in a superconducting qubit, *Physical Review Letters* **130**, 267001 (2023).
- [9] L. Ding, M. Hays, Y. Sung, B. Kannan, J. An, A. Di Paolo, A. H. Karamlou, T. M. Hazard, K. Azar, D. K. Kim, *et al.*, High-fidelity, frequency-flexible two-qubit fluxonium gates with a transmon coupler, *Physical Review X* **13**, 031035 (2023).
- [10] J. Koch, M. Y. Terri, J. Gambetta, A. A. Houck, D. I. Schuster, J. Majer, A. Blais, M. H. Devoret, S. M. Girvin, and R. J. Schoelkopf, Charge-insensitive qubit design derived from the cooper pair box, *Physical Review A* **76**, 042319 (2007).
- [11] J. A. Schreier, A. A. Houck, J. Koch, D. I. Schuster, B. R. Johnson, J. M. Chow, J. M. Gambetta, J. Majer, L. Frunzio, M. H. Devoret, *et al.*, Suppressing charge noise decoherence in superconducting charge qubits, *Physical Review B* **77**, 180502 (2008).
- [12] H. Paik, D. I. Schuster, L. S. Bishop, G. Kirchmair, G. Catelani, A. P. Sears, B. Johnson, M. Reagor, L. Frunzio, L. I. Glazman, *et al.*, Observation of high coherence in josephson junction qubits measured in a three-dimensional circuit qed architecture, *Physical Review Letters* **107**, 240501 (2011).
- [13] V. E. Manucharyan, J. Koch, L. I. Glazman, and M. H. Devoret, Fluxonium: Single cooper-pair circuit free of charge offsets, *Science* **326**, 113 (2009).
- [14] J. Koch, V. Manucharyan, M. Devoret, and L. Glaz-

- man, Charging effects in the inductively shunted josephson junction, *Physical review letters* **103**, 217004 (2009).
- [15] V. E. Manucharyan, N. A. Masluk, A. Kamal, J. Koch, L. I. Glazman, and M. H. Devoret, Evidence for coherent quantum phase slips across a josephson junction array, *Physical Review B* **85**, 024521 (2012).
- [16] L. B. Nguyen, G. Koolstra, Y. Kim, A. Morvan, T. Chistolini, S. Singh, K. N. Nesterov, C. Jünger, L. Chen, Z. Pedramrazi, *et al.*, Blueprint for a high-performance fluxonium quantum processor, *PRX Quantum* **3**, 037001 (2022).
- [17] J. M. Martinis, K. B. Cooper, R. McDermott, M. Steffen, M. Ansmann, K. Osborn, K. Cicak, S. Oh, D. P. Pappas, R. W. Simmonds, *et al.*, Decoherence in josephson qubits from dielectric loss, *Physical review letters* **95**, 210503 (2005).
- [18] C. Wang, C. Axline, Y. Y. Gao, T. Brecht, Y. Chu, L. Frunzio, M. Devoret, and R. J. Schoelkopf, Surface participation and dielectric loss in superconducting qubits, *Applied Physics Letters* **107** (2015).
- [19] J. M. Gambetta, C. E. Murray, Y.-K.-K. Fung, D. T. McClure, O. Dial, W. Shanks, J. W. Sleight, and M. Steffen, Investigating surface loss effects in superconducting transmon qubits, *IEEE Transactions on Applied Superconductivity* **27**, 1 (2016).
- [20] I. Siddiqi, Engineering high-coherence superconducting qubits, *Nature Reviews Materials* **6**, 875 (2021).
- [21] F. Yan, S. Gustavsson, A. Kamal, J. Birenbaum, A. P. Sears, D. Hover, T. J. Gudmundsen, D. Rosenberg, G. Samach, S. Weber, *et al.*, The flux qubit revisited to enhance coherence and reproducibility, *Nature communications* **7**, 12964 (2016).
- [22] P. Klimov, J. Kelly, Z. Chen, M. Neeley, A. Megrant, B. Burkett, R. Barends, K. Arya, B. Chiaro, Y. Chen, *et al.*, Fluctuations of energy-relaxation times in superconducting qubits, *Physical review letters* **121**, 090502 (2018).
- [23] A. P. Place, L. V. Rodgers, P. Mundada, B. M. Smitham, M. Fitzpatrick, Z. Leng, A. Premkumar, J. Bryon, A. Vrajitoarea, S. Sussman, *et al.*, New material platform for superconducting transmon qubits with coherence times exceeding 0.3 milliseconds, *Nature communications* **12**, 1779 (2021).
- [24] A. Osman, J. Simon, A. Bengtsson, S. Kosen, P. Krantz, D. P. Lozano, M. Scigliuzzo, P. Delsing, J. Bylander, and A. Fadavi Roudsari, Simplified josephson-junction fabrication process for reproducibly high-performance superconducting qubits, *Applied Physics Letters* **118** (2021).
- [25] C. Wang, X. Li, H. Xu, Z. Li, J. Wang, Z. Yang, Z. Mi, X. Liang, T. Su, C. Yang, *et al.*, Towards practical quantum computers: Transmon qubit with a lifetime approaching 0.5 milliseconds, *npj Quantum Information* **8**, 3 (2022).
- [26] S. Kono, J. Pan, M. Chegnizadeh, X. Wang, A. Youssefi, M. Scigliuzzo, and T. J. Kippenberg, Mechanically induced correlated errors on superconducting qubits with relaxation times exceeding 0.4 milliseconds, *arXiv preprint arXiv:2305.02591* (2023).
- [27] N. Earnest, S. Chakram, Y. Lu, N. Irons, R. K. Naik, N. Leung, L. Ocola, D. A. Czaplowski, B. Baker, J. Lawrence, *et al.*, Realization of a λ system with metastable states of a capacitively shunted fluxonium, *Physical review letters* **120**, 150504 (2018).
- [28] B.-L. Najera-Santos, R. Rousseau, K. Gerashchenko, H. Patange, A. Riva, M. Villiers, T. Briant, P.-F. Cohadon, A. Heidmann, J. Palomo, *et al.*, High-sensitivity ac-charge detection with a mhz-frequency fluxonium qubit, *Physical Review X* **14**, 011007 (2024).
- [29] L. Ioffe and M. Feigel'man, Possible realization of an ideal quantum computer in josephson junction array, *Physical Review B* **66**, 224503 (2002).
- [30] A. Kitaev, Protected qubit based on a superconducting current mirror, *arXiv preprint cond-mat/0609441* (2006).
- [31] P. Brooks, A. Kitaev, and J. Preskill, Protected gates for superconducting qubits, *Physical Review A* **87**, 052306 (2013).
- [32] J. Kreikebaum, K. O'Brien, A. Morvan, and I. Siddiqi, Improving wafer-scale josephson junction resistance variation in superconducting quantum coherent circuits, *Superconductor Science and Technology* **33**, 06LT02 (2020).
- [33] P. Groszkowski, A. D. Paolo, A. Grimsmo, A. Blais, D. Schuster, A. A. Houck, and J. Koch, Coherence properties of the $0-\pi$ qubit, *New Journal of Physics* **20**, 043053 (2018).
- [34] A. Gyenis, A. Di Paolo, J. Koch, A. Blais, A. A. Houck, and D. I. Schuster, Moving beyond the transmon: Noise-protected superconducting quantum circuits, *PRX Quantum* **2**, 030101 (2021).
- [35] A. Gyenis, P. S. Mundada, A. Di Paolo, T. M. Hazard, X. You, D. I. Schuster, J. Koch, A. Blais, and A. A. Houck, Experimental realization of a protected superconducting circuit derived from the $0-\pi$ qubit, *PRX Quantum* **2**, 010339 (2021).
- [36] K. Kalashnikov, W. T. Hsieh, W. Zhang, W.-S. Lu, P. Kamenov, A. Di Paolo, A. Blais, M. E. Gershenson, and M. Bell, Bifluxon: Fluxon-parity-protected superconducting qubit, *PRX Quantum* **1**, 010307 (2020).
- [37] W.-L. Ma, S. Puri, R. J. Schoelkopf, M. H. Devoret, S. Girvin, and L. Jiang, Quantum control of bosonic modes with superconducting circuits, *Science Bulletin* **66**, 1789 (2021).
- [38] A. Joshi, K. Noh, and Y. Y. Gao, Quantum information processing with bosonic qubits in circuit qed, *Quantum Science and Technology* **6**, 033001 (2021).
- [39] D. Vion, D. Esteve, and M. Devoret, Quantum coherence with a single cooper pair, *Physica Scripta* **1998**, 165 (1998).
- [40] R. A. Mencia, *Ultra-high impedance superconducting circuits*, Ph.D. thesis, University of Maryland, College Park (2023).
- [41] K. Matveev, A. Larkin, and L. Glazman, Persistent current in superconducting nanorings, *Physical review letters* **89**, 096802 (2002).
- [42] P. Krantz, M. Kjaergaard, F. Yan, T. P. Orlando, S. Gustavsson, and W. D. Oliver, A quantum engineer's guide to superconducting qubits, *Applied physics reviews* **6** (2019).
- [43] G. Zhu, D. G. Ferguson, V. E. Manucharyan, and J. Koch, Circuit qed with fluxonium qubits: Theory of the dispersive regime, *Physical Review B* **87**, 024510 (2013).
- [44] J. M. Martinis, K. B. Cooper, R. McDermott, M. Steffen, M. Ansmann, K. D. Osborn, K. Cicak, S. Oh, D. P. Pappas, R. W. Simmonds, and C. C. Yu, Decoherence in Josephson Qubits from Dielectric Loss, *Physical Review Letters* **95**, 210503 (2005), *cond-mat/0507622*.
- [45] A. Megrant, C. Neill, R. Barends, B. Chiaro, Y. Chen,

- L. Feigl, J. Kelly, E. Lucero, M. Mariani, P. J. J. O'Malley, D. Sank, A. Vainsencher, J. Wenner, T. C. White, Y. Yin, J. Zhao, C. J. Palmström, J. M. Martinis, and A. N. Cleland, Planar superconducting resonators with internal quality factors above one million, *Applied Physics Letters* **100**, 113510 (2012), 1201.3384.
- [46] C. Wang, C. Axline, Y. Y. Gao, T. Brecht, Y. Chu, L. Frunzio, M. H. Devoret, and R. J. Schoelkopf, Surface participation and dielectric loss in superconducting qubits, *Applied Physics Letters* **107**, 162601 (2015), 1509.01854.
- [47] A. Kamal, J. L. Yoder, F. Yan, T. J. Gudmundsen, D. Hover, A. P. Sears, P. Welander, T. P. Orlando, S. Gustavsson, and W. D. Oliver, Improved superconducting qubit coherence with high-temperature substrate annealing, *arXiv* (2016), 1606.09262.
- [48] A. Nersisyan, S. Poletto, N. Alidoust, R. Manenti, R. Renzas, C.-V. Bui, K. Vu, T. Whyland, Y. Mohan, E. A. Sete, S. Stanwyck, A. Bestwick, and M. Reagor, Manufacturing low dissipation superconducting quantum processors, *arXiv* 10.1109/iedm19573.2019.8993458 (2019), 1901.08042.
- [49] A. P. M. Place, L. V. H. Rodgers, P. Mundada, B. M. Smitham, M. Fitzpatrick, Z. Leng, A. Premkumar, J. Bryon, A. Vrajitoarea, S. Sussman, G. Cheng, T. Madhavan, H. K. Babla, X. H. Le, Y. Gang, B. Jäck, A. Geynis, N. Yao, R. J. Cava, N. P. d. Leon, and A. A. Houck, New material platform for superconducting transmon qubits with coherence times exceeding 0.3 milliseconds, *Nature Communications* **12**, 1779 (2021), 2003.00024.
- [50] W. Smith, A. Kou, U. Vool, I. Pop, L. Frunzio, R. Schoelkopf, and M. Devoret, Quantization of inductively shunted superconducting circuits, *Physical Review B* **94**, 144507 (2016).
- [51] A. Kou, W. Smith, U. Vool, I. Pop, K. Sliwa, M. Hatridge, L. Frunzio, and M. Devoret, Simultaneous monitoring of fluxonium qubits in a waveguide, *Physical Review Applied* **9**, 064022 (2018).
- [52] I. V. Pechenezhskiy, R. A. Mencia, L. B. Nguyen, Y.-H. Lin, and V. E. Manucharyan, The superconducting quasicharge qubit, *Nature* **585**, 368 (2020).
- [53] N. Cottet, H. Xiong, L. B. Nguyen, Y.-H. Lin, and V. E. Manucharyan, Electron shelving of a superconducting artificial atom, *Nature communications* **12**, 6383 (2021).
- [54] I. M. Pop, K. Geerlings, G. Catelani, R. J. Schoelkopf, L. I. Glazman, and M. H. Devoret, Coherent suppression of electromagnetic dissipation due to superconducting quasiparticles, *Nature* **508**, 369 (2014).
- [55] S. Lazăr, Q. Ficheux, J. Herrmann, A. Remm, N. Lacroix, C. Hellings, F. Swiadek, D. C. Zanuz, G. J. Norris, M. B. Panah, *et al.*, Calibration of drive nonlinearity for arbitrary-angle single-qubit gates using error amplification, *Physical Review Applied* **20**, 024036 (2023).
- [56] J. R. Johansson, P. D. Nation, and F. Nori, Qutip: An open-source python framework for the dynamics of open quantum systems, *Computer Physics Communications* **183**, 1760 (2012).
- [57] L. H. Pedersen, N. M. Møller, and K. Mølmer, Fidelity of quantum operations, *Physics Letters A* **367**, 47 (2007).